Ab initio Molecular Dynamical Investigation of the Finite Temperature Behavior of the Tetrahedral Au$_{19}$ and Au$_{20}$ Clusters.

Sailaja Krishnamurty* and Ghazal S. Shafai and D. G. Kanhere

Department of Physics and Centre for Modeling and Simulation,
University of Pune, Ganeshkhind, Pune–411 007, India

B. Soulé de Bas and M. J. Ford

Institute for Nanoscale Technology, University of Technology,
Sydney PO Box 123, Broadway, NSW 2007 Australia

Density functional molecular dynamics simulations have been carried out to understand the finite temperature behavior of Au$_{19}$ and Au$_{20}$ clusters. Au$_{20}$ has been reported to be a unique molecule having tetrahedral geometry, a large HOMO-LUMO energy gap and an atomic packing similar to that of the bulk gold (J. Li et al., Science, **299** 864, 2003). Our results show that the geometry of Au$_{19}$ is exactly identical to that of Au$_{20}$ with one missing corner atom (called as vacancy). Surprisingly, our calculated heat capacities for this nearly identical pair of gold cluster exhibit dramatic differences. Au$_{20}$ undergoes a clear and distinct solid like to liquid like transition with a sharp peak in the heat capacity curve around 770 K. On the other hand, Au$_{19}$ has a broad and flat heat capacity curve with continuous melting transition. This continuous melting transition turns out to be a consequence of a process involving series of atomic rearrangements along the surface to fill in the missing corner atom. This results in a restricted diffusive motion of atoms along the surface of Au$_{19}$ between 650 K to 900 K during which the shape of the ground state geometry is retained. In contrast, the tetrahedral structure of Au$_{20}$ is destroyed around 800 K, and the cluster is clearly in a liquid like state above 1000 K. Thus, this work clearly demonstrates that (i) the gold clusters exhibit size sensitive variations in the heat capacity curves and (ii) the broad and continuous melting transition in a cluster, a feature which has so far been attributed to the disorder or absence of symmetry in the system, can also be a consequence of a defect (absence of a cap atom) in the structure.

I. INTRODUCTION

Recently discovered clusters and nanostructures of gold are found to have a rich chemistry with potential applications in materials science,[1] medicine,[2] and in the area of catalysis.[3,4] In particular, small clusters of gold have attracted interest as tips and contacts in molecular electronic circuits[5] and also as chemical catalysts.[6] Experimentally, even a small cluster such as Au$_8$ has been reported to catalyze the oxidation reaction of CO.[7] However, these properties are reported to have strong size sensitive variations. Another factor influencing the application of gold clusters is their thermal stability. It is noted that several Au clusters undergo structural transformation or tend to grow readily by migrating and merging[8] under high-temperature conditions (500 K and above). These effects have important consequences in the applications involving elevated temperatures and the growth mechanisms of clusters. In this context, a study on the finite temperature behavior of Au clusters is of considerable importance.

Since the pioneering reports on the possible applications of gold clusters, a large amount of experimental[9] and theoretical works[10] have been devoted to understand the structural and electronic properties of Au$_n$ (n ≤ 50) clusters. These reports have demonstrated that gold clusters have very different physical and chemical properties as compared to their bulk counterpart. A more recent exciting report has shown photo electron spectroscopic evidence of hollow golden cages with an average diameter of 5.5 Å in the in the size range of 16 to 18 atoms.[11] These predictions were further supported by the theoretical calculations in the same report. However, Au$_{20}$ is the most intriguing gold cluster reported so far.[12] Experimental studies[11,12] report this cluster to have a pyramidal structure (tetrahedral symmetry) with each of the four faces representing the (111) surface of the Face Centered Cubic (FCC) gold. It is reported to have a large energy gap between the Highest Occupied Molecular Orbital (HOMO) and Lowest Occupied Molecular Orbital (LUMO). This energy gap is greater than that of C$_{60}$ suggesting it to be highly stable and chemically inert. On the other hand, its structure with high surface area and large fraction of corner sites with low atomic coordination is expected to provide ideal surface sites to bind various molecules such as CO, O$_2$ and CO$_2$ for catalysis. The structure of Au$_{19}$ is also seen to be very similar to that of Au$_{20}$ with one missing corner atom. In this context, it is interesting to have an understanding on the thermal stability of these two gold clusters having an atomic packing similar to that of bulk gold. Hence, in the present work, we study the finite temperature behavior of Au$_{19}$ and Au$_{20}$ using the first principles Molecular Dynamics (MD) simulations.

While several experimental and theoretical studies have been devoted to understand the ground state geometries and chemical reactivity of gold clusters, there are very few reports on the finite temperature properties of gold clusters.[13,14] The classical MD simulations by

Landman and co-workers[13,14] on medium sized Au clusters (150-1500 atoms) indicated that the clusters in this size range undergo a solid–to–solid structural transformation around 700 K, before eventually melting around 780 K. This is at a much lower value as compared to the bulk melting temperature of 1377 K. However, to the best of our knowledge, only one ab initio molecular dynamics study[15] attempting to understand the finite temperature behavior of Au clusters has been reported so far.

As the cluster size reduces, the electronic effects play a more explicit role in controlling the structural and thermal properties of the clusters. This is amply demonstrated by several first principles molecular dynamics simulations,[16–24] which have successfully explained various experimental findings[25–33] on the finite temperature behavior of sodium, tin, gallium and aluminum clusters. These experimental studies have brought out various interesting phenomena such as higher than bulk melting temperatures in Ga and Sn clusters,[29,30] and strong size dependent variations in the melting temperatures of Ga and Al clusters.[31,32] However, the most surprising experimental finding is the size sensitive behavior of the shape of the heat capacities where addition of even one atom is seen to result in a dramatic change of shape, prompting some of the clusters to be called as "Magic Melters".[31] This means that while some clusters do undergo a conventional and clear melting transition, others undergo a near continuous transition making it very difficult to identify any meaningful transition temperature. In a recent communication,[17] we have clearly demonstrated that a cluster with local "order" (an island of atoms connected with equal bond strengths) displays a well characterized melting transition with a distinct peak in the heat capacity curve, while a "disordered" cluster is seen to undergo a continuous transition with a flat heat capacity curve. Further, it is noted that this size sensitive nature in small clusters is related to the evolutionary pattern seen in their ground states and is seen to exist in clusters of sodium, gallium and aluminum.[24,34,35]

In what follows, we show that this dramatic variation in the shape of heat capacity curve is also observed in the present pair of gold clusters viz., Au_{19} and Au_{20}. This observation has also thrown light on additional factors responsible for a continuous melting transition in clusters. As we shall see, in contrast to gallium or aluminum clusters, the flat or broad heat capacity curve in Au_{19} is attributed to a "vacancy" in the surface (or a surface defect). This "vacancy" results in a chain of atomic rearrangements leading to a restricted diffusion of atoms along the surface. In contrast, Au_{20} undergoes a relatively sharp melting transition with a clear peak in the heat capacity curve around 770 K. Thus, these results not only bring out an understanding on additional factors contributing to the broad melting transition in clusters but also on the relative thermal stability of these unique tetrahedral gold clusters.

II. COMPUTATIONAL DETAILS

We have optimized about 300 geometries for each of the cluster, to obtain the ground state geometry and several low energy isomers. The initial configurations for the optimization were obtained by carrying out a constant temperature dynamics of 100 ps each at various temperatures between 400 to 1600 K. Once the ground state geometry is obtained, thermodynamic simulations are performed using Born–Oppenheimer MD based on the Kohn-Sham formulation of Density Functional Theory (DFT).[36] The ionic phase space of the clusters is sampled classically in a canonical ensemble according to the method proposed by Nóse.[37] The mass of the Nóse thermostat is chosen such that the characteristic frequency of the thermostat falls within the range of the vibrational eigen frequencies of the system. The potential energy distribution obtained by the Nóse thermostat with this mass is further seen to be statistically similar to the one generated by using an isokinetic velocity scaling algorithm[38]. The MD simulations have been carried out using Vanderbilt's ultra soft pseudo potentials[39] within the Local Density Approximation (LDA) for describing the core-valance interactions as implemented in the vasp package.[40] The ground state geometry and low lying isomers of both the clusters using LDA and Generalized Gradient Approximation (GGA) are seen to be very similar to each other. The energy differences between the isomers in LDA are found to be within a few % of those obtained by GGA. Energy cutoff of 13.21 Ry is used for the plane wave expansion of Au. We have used cubic super cells of length 20 Å and have ensured that the results converge with respect to further increase in the energy cutoff and size of the simulation box.

Following the finite temperature study, the ionic heat capacity of both the clusters is computed using the multiple histogram (MH) method.[42,43] The computation of the heat capacity using the MH technique is sensitive to the number of temperatures at which the thermodynamic behavior of the cluster is simulated. The range and the number of temperatures must be chosen so as to have an adequate overlap of potential energy distribution. In order to have a reliable sampling, we split the total temperature range from 400–1600 K into at least 15 different temperatures for both clusters. We maintain the cluster at each temperature for a period of at least 100 ps after equilibration, leading to a total simulation time of around 1 ns. We have further ensured that our heat capacity curve does not change with the addition of further temperatures between 400-1600 K. The MH method and the various errors associated with it are discussed in detail in one of the earlier works.[20]

An important source of error in MD simulations in the limited statistics for calculating the finite temperature properties. It may be noted that the *ab initio* nature of the method puts restriction on the simulation time scales. As examination of the convergence of various thermodynamic indicators, has indicated that a simulation time of

70 ps is sufficient enough in the present case. During the MD simulations, the small amount of angular momentum of the clusters is removed from the equation of the ionic motion at every step. Another way to remove the angular momentum from the clusters is described in one of the recent works.[41].

Various other thermodynamic indicators such as the mean-square displacements (MSD)'s of ions and the root-mean-square bond-length fluctuation (RMS-BLF or $\delta_{\rm rms}$) are also computed. For the sake of completeness we briefly discuss these parameters. The parameter $\delta_{\rm rms}$ is a measure of the fluctuations in the bond lengths averaged over all the atoms and over the total time span. It is defined as

$$\delta_{\rm rms} = \frac{2}{N(N-1)} \sum_{i>j} \frac{(\langle r_{ij}^2 \rangle_t - \langle r_{ij} \rangle_t^2)^{1/2}}{\langle r_{ij} \rangle_t}, \qquad (1)$$

where N is the number of atoms in the system, r_{ij} is the distance between atoms i and j, and $\langle \ldots \rangle_t$ denotes a time average over the entire trajectory. The MSD is another widely used parameter for analyzing a solid-like-to-liquid-like transition. In the present work, we calculate the mean square displacement's for individual atoms which is defined as

$$\langle \mathbf{r}_I^2(t) \rangle = \frac{1}{M} \sum_{m=1}^{M} [\mathbf{R}_I(t_{0m}+t) - \mathbf{R}_I(t_{0m})]^2, \qquad (2)$$

where $\mathbf{R}_I$ is the position of the Ith atom and we average over M different time origins t_{0m} spanning the entire trajectory. The MSD indicates the displacement of atom in the cluster as a function of time. In the solid-like region, all atoms perform oscillatory motion about fixed points resulting in a negligible MSD's of individual atoms from their equilibrium positions. In a liquid-like state, on the other hand, atoms diffuse throughout the cluster and the MSD's eventually reach a saturated value of the order of the square of the cluster radius. More technical details concerning the extraction of thermodynamic averages, indicators and computation of the heat capacity curve can be found in previous work.[43]

III. RESULTS AND DISCUSSION

We begin with a discussion on the ground state geometries and some representative low lying isomers of Au$_{19}$ and Au$_{20}$ which are shown in the Fig. 1 and Fig. 2, respectively. It is clearly seen from these figures that the ground state geometry of Au$_{20}$ (Fig. 2–(a)) is a tetrahedron. The ground state geometry of Au$_{19}$ (Fig. 1–(a)) differs from that of Au$_{20}$ by a single missing vertex atom of the tetrahedron. This is in agreement with the recent experimental and theoretical predictions.[11] Quite clearly both the structures are symmetric, with ordered triangles stacked over one another. The rest of the geometric parameters such as bond lengths, bond angles and dihedral angles are almost identical in both the ground state
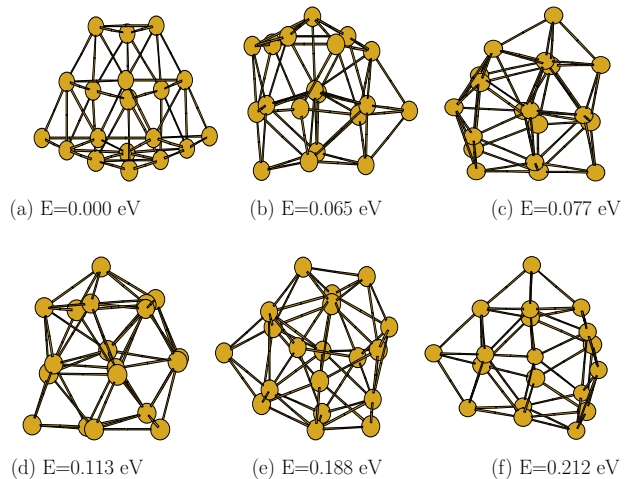

(a) E=0.000 eV (b) E=0.065 eV (c) E=0.077 eV

(d) E=0.113 eV (e) E=0.188 eV (f) E=0.212 eV

FIG. 1: The ground state geometry and low lying isomers of Au$_{19}$. The energy below is the difference in total energy of the isomer with respect to the ground state energy.

geometries. Thus, Au$_{19}$ can be considered as Au$_{20}$ with a vertex defect.

The atoms in Au$_{19}$ as well as Au$_{20}$ are bonded to their first nearest neighbors with bond distances of either 2.63 Å (shortest bonds in the cluster) or 2.75 Å (next shortest bonds). It is interesting to display the connectivity of the shortest bonds to bring out the differences in them. Fig. 3–(a) and Fig. 3–(b) show the distribution of shortest bonds (2.63 Å) for the case of Au$_{19}$ and Au$_{20}$, respectively. Clearly, the shortest bonds are distributed only along the surface of both the clusters and form a closed network in Au$_{20}$, while in Au$_{19}$ they form an open network due to the missing atom. It turns out, that the presence of the vertex defect and open skeleton of shortest bonds in Au$_{19}$ play a significant role in the finite temperature behavior of the cluster around 650 K and initiate a set of restricted atomic rearrangements on the surface.

The low lying isomers of Au$_{19}$ (shown in Fig. 1–(b) to Fig. 1–(f)) are clearly devoid of a regular triangular arrangement of atoms seen in the ground state configuration. The first low lying isomer of Au$_{19}$ (Fig. 1–(b)) is nearly 0.065 eV higher in energy as compared to the ground state configuration. Au$_{19}$ has several isomers with continuous energy distribution between 0.065 eV to 0.7 eV some of which are shown in Fig. 1–(c) to Fig. 1–(f). This can be contrasted with first low lying isomer of Au$_{20}$ (shown in Fig. 2–(b)) which is almost 0.44 eV higher than the ground state geometry. This structure has one central atom and rest of the 19 atoms arrange around this central atom so as to have a highly deformed tetrahedron. This configuration is degenerate with the hollow cage configuration of Au$_{20}$ (Fig. 2–(c)). The fact that there are a couple of isomers well separated from the ground state geometry correlates very well with the existence of a relatively sharp and well defined peak in the heat capacity curve of Au$_{20}$. Some other representative

(a) E=0.000 eV   (b) E=0.444 eV   (c) E=0.445 eV
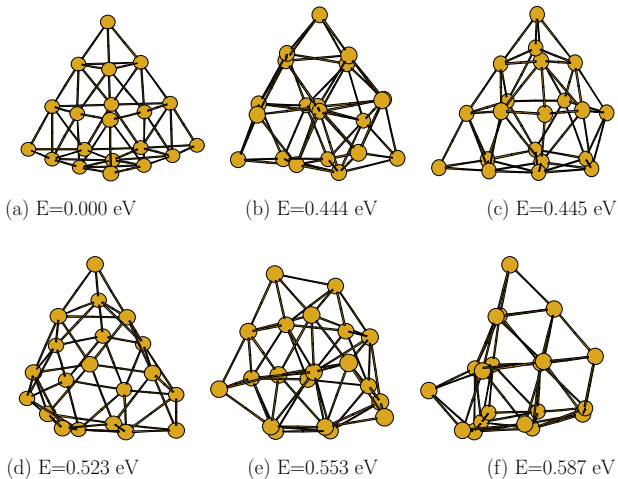
(d) E=0.523 eV   (e) E=0.553 eV   (f) E=0.587 eV

FIG. 2: The ground state geometry and low lying isomers of Au_{20}. The energy below is the difference in total energy of the isomer with respect to the ground state energy.

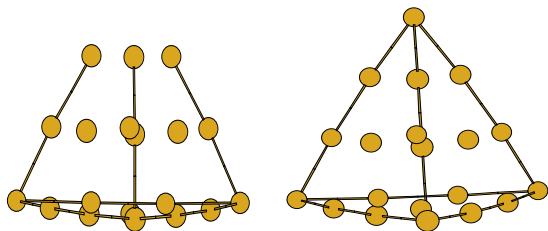FIG. 3: The distribution of shortest bonds (2.63 Å) in Au_{19} and Au_{20}. Rest of the inter atomic bond distances (for the first nearest nearest neighbor) in both the clusters are 2.75 Å.

FIG. 4: The Heat-Capacity Curves of Au_{19} and Au_{20}. C_0 = $(3N-9/2)K_B$ is the zero-temperature classical limit of the rotational plus vibrational canonical specific heat. The bar at the peak of Au_{20} curve indicates the maximum estimated error in the height. The peak positions are stable to within $\pm$ 50 K.

low lying isomers of Au_{20} are shown in Fig. 2–(d) to Fig. 2–(f). We also note that the atoms in all the high energy configurations of both clusters are bonded to each other through a much wider and continuous range of Au-Au bond lengths (ranging between 2.67 Å-2.90 Å) as compared to those in the ground state geometry.

Now, we present the finite temperature behavior of both the clusters. we begin with a discussion on the calculated heat capacity curves which is shown in Fig. 4. The figure brings out a remarkable feature, viz., a significant size sensitivity nature of the heat capacity curves. The heat capacity curve of Au_{20} has a clear and recognizable peak around 770 K, with a width of about 250 K. In contrast, the heat-capacity curve of Au_{19}, a cluster with a vacancy, shows a broad and almost continuous solid–to–liquid transition between 650 K–1200 K. Thus, this is yet an another example of dramatic change in the shape of the heat capacity curve with the addition of a single atom. As already noted this size sensitive nature has been observed earlier in Ga, Al clusters experimentally.[31,32]

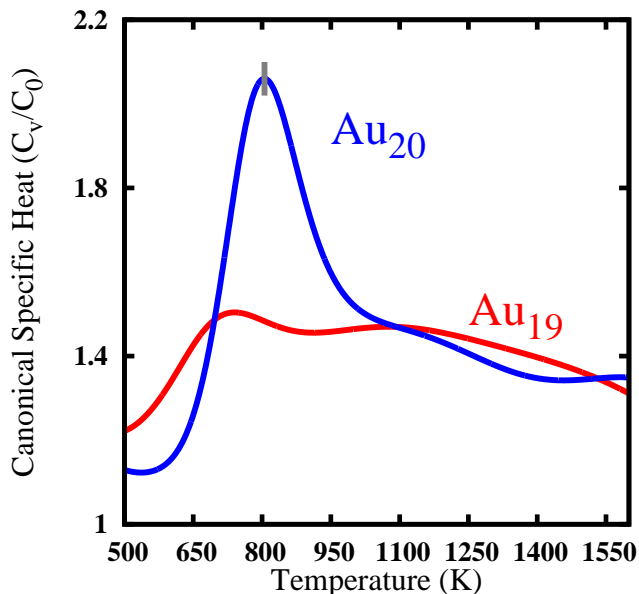It is possible to make a detailed analysis of the ionic motion by examining the trajectories of the clusters. An analysis of the ionic motions of Au_{19} reveals the cluster to vibrate around its ground state geometry until 600 K. Around 650 K, the cluster undergoes a peculiar structural rearrangement so as to fill in the vacancy (the apex atom). The snapshots of this structural rearrangement are shown from Fig. 5–(a) to Fig. 5–(e). Fig. 5–(a) shows Au_{19} with a missing cap atom. Note that, at the end of the structural rearrangement (Fig. 5–(e)), the vacancy which is present on the top in Fig. 5–(a) is shifted to the bottom edge. We denote the edge consisting of atoms 'A', 'B' and 'C' as the reference edge. Coming to the details of the structural rearrangement, as the cluster evolves around 650 K, it is seen that these atoms in the reference edge push themselves upward (see Fig. 5–(b) to Fig. 5–(d)). The rest of atoms in the cluster undergo minor displacements around their equilibrium positions during this process. At the end of this rearrangement (see Fig. 5–(e)), it is seen that the top edge atom (atom 'C') in Au_{19} moves to cap the missing vertex atom seen in Fig. 5–(a). The next edge atom ('B') moves up to occupy the position initially occupied by atom 'C' and atom the 'A' occupies the position occupied by 'B'. Now this creates a vacancy or defect at the position initially occupied by the atom 'A'. Thus, we now have a Au_{19} cluster which is rotated by 90 degrees in the anti clock wise direction (Fig. 5–(e)) with respect to Fig. 5–(a).

Around 650 K, only a single edge is displaced so as to cap the missing vertex atom. Between 700 K–900 K, we see a continuous displacement of atoms along all the
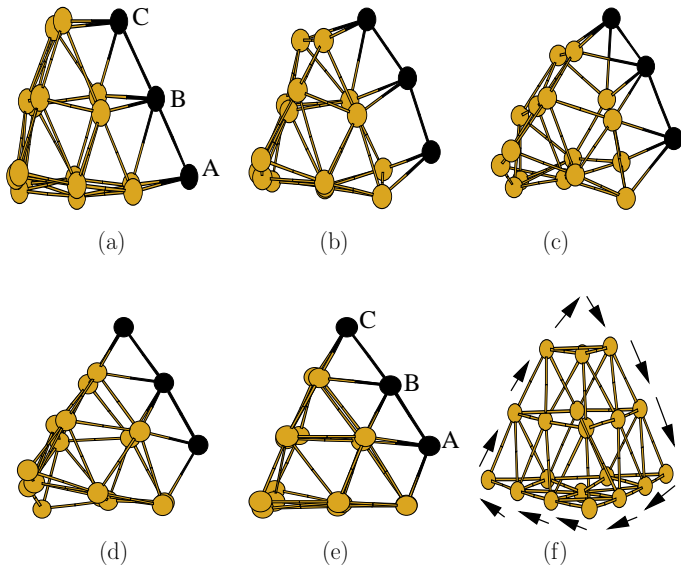
FIG. 5: (a–e) Snapshots of restricted rearrangement of atoms in Au_{19} around 650 K. (f) Arrows depict the continuous atomic rearrangements that take place to fill in the missing cap atom between 700 K–900 K.

edges as shown in Fig. 5–(f) as the vacancy is shifted from one vertex to the other vertex. A remarkable feature of this motion is that the overall shape of the cluster remains approximately tetrahedron with a missing cap. Around 1000 K, the tetrahedron structure is destroyed and the cluster visits its first and second high energy configurations. The cluster finally melts completely above 1200 K. This leads to a broad feature (between 650 K–1200 K) in its heat capacity curve.

In contrast, the ionic motion of Au_{20} shows all the atoms to vibrate around their initial positions until about 750 K. The cluster undergoes a structural transformation from the ground state geometry to the first isomer shown in Fig. 2–(b) around 800 K. The cluster visits other isomers around 900 K and melts completely above 1000 K leading to a clear and relatively narrow melting transition.

This contrasting behavior is brought out more clearly by examining the MSD's of the individual atoms. **It may be recalled that we have ensured that our clusters do not rotate and hence, the MSD values that we report correspond to the absolute displacement of the ion from its original position.** In Fig. 6, we show the MSD's of individual atoms in both clusters in the temperature range of 450 K–1000 K. It is clearly from Fig. 6–(a) and Fig. 6–(b) that atoms in both the clusters vibrate around their equilibrium positions at 450 K. Around 650 K, the rearrangement of atoms along one edge in Au_{19} is reflected in slightly higher mean square displacements (around 3 Å) in Fig. 6–(c). These values increase continuously in Au_{19} as shown by the typical behavior around 800 K. In contrast, the MSD values in Au_{20} are negligible until 750 K (< 0.5 Å) and the val-
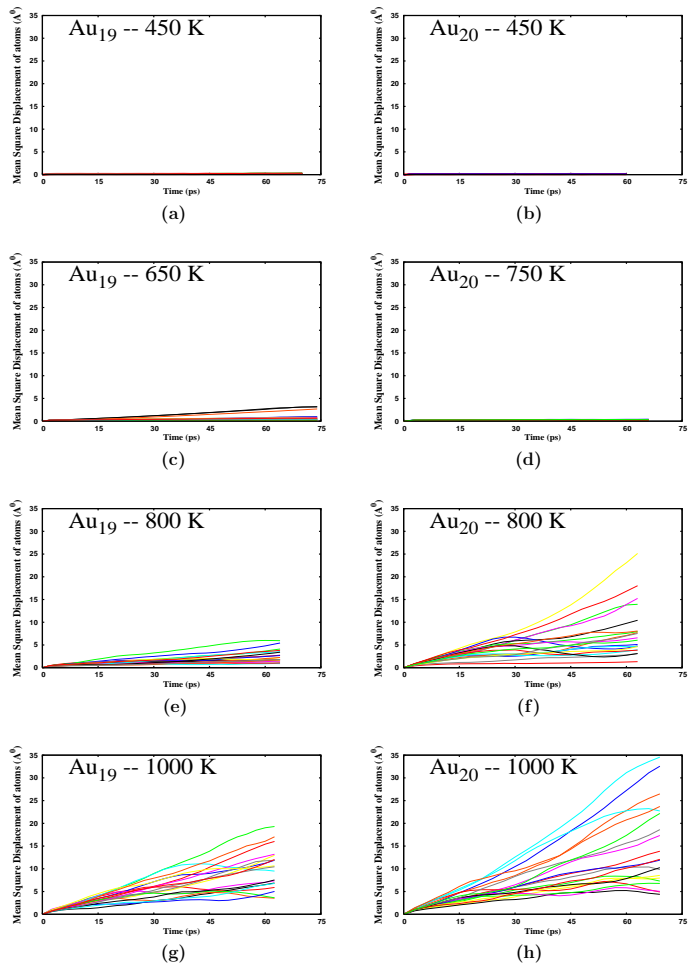
FIG. 6: The Root Mean Square Displacements of atoms with respect to the simulation time (ps) in Au_{19} at various temperatures.

ues increase sharply around 800 K. It is precisely at this temperature that the tetrahedron gets destroyed. The MSD's of Au_{19} and Au_{20} saturate around 35 Å at 1200 K and 1000 K respectively indicating the presence of a liquid like state.

This contrasting behavior is some what weakly reflected in in average root-mean-square bond-length fluctuation (δ_{rms}) of Au_{19} and Au_{20}, which is in any case a quantity averaged out over all the atoms. In Fig. 7 we show the δ_{rms} for both the clusters. As expected Au_{20} shows a sharp transition indicated by a jump in δ_{rms} value from 0.07 to 0.20.

IV. SUMMARY AND CONCLUSIONS

In this work, we have presented the results of first principle molecular dynamics simulations on Au_{19} and Au_{20}, clusters which have atomic packing similar to that of the bulk gold. In spite of the fact, that the geometry of both the clusters is nearly identical except for a single vertex
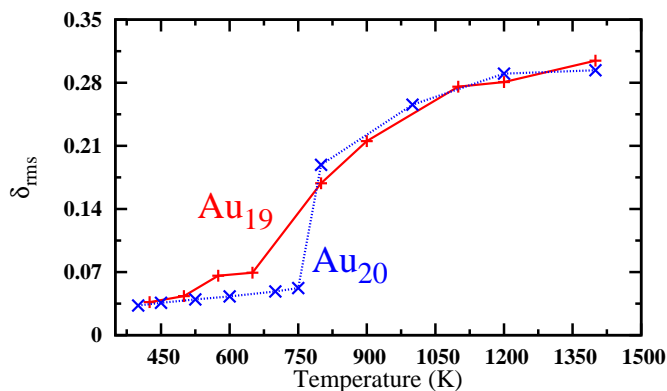
FIG. 7: δ_{rms} of Au$_{19}$ and Au$_{20}$.

nature of the heat capacity curves has been observed experimentally in Al and Ga clusters and in Na clusters during the ab initio molecular dynamic simulations. In these studies the size sensitive nature of the heat capacity curves was attributed to the nature of the "disorder" in the ground state geometry. The present work clearly shows that this size sensitive behavior is also driven by the vacancy in the other wise perfect and symmetric "lattice". The work also demonstrates that the size sensitive variations in the melting characteristics to be generic in nature. Finally, the contrasting finite temperature behavior reported in the present gold clusters could have several implications in the applications of these clusters and is a topic of further research interest.

Acknowledgments

atom, they exhibit dramatic differences in the shape of their heat capacity curves. We have shown that these differences are induced by vacancy. The vacancy in Au$_{19}$ induces a restricted diffusive motion along the surface of the cluster leading to a continuous melting transition. In contrast, Au$_{20}$ exhibits a sudden and clear melting transition. It may be noted that such a size sensitive

* Electronic address: `sailaja@unipune.ernet.in`
[1] Dyson, P. J.; Mingos, D. M. P. *Gold. Progress in Chemistry, Biochemistry and Technology* (ed. Schmidbaur, H.), Wiley, Newyork, **1999**, 511.
[2] Shaw III, C. F. *Chem. Rev.* **1999**, 99, 2589.
[3] Teles, J. H.; Brode, S.; Chabanas, M. *Angew. Chem.* **1998**, 99, 2589.
[4] Hashmi, A. S. K. *Gold Bull.* **2003**, 36, 3.
[5] Fan, F.-R. F.; Bard, A. J. *Science* **1997**, 277, 1791.
[6] Valden, M.; Lai, X.; Landman, D. W. *Science* **1998**, 281, 1647.
[7] Pyykko, P. *Angew. Chem. Int. Ed.* **2004**, 43, 4412.
[8] Sutter, E.; Sutter, P.; Zhu, Y. *Nano Letters* **2005**, 5, 2092.
[9] Gilb, S.; Weis, P.; Furche, F.; Ahlrichs, R.; Kappes, M. M. *J. Chem. Phys.* **2002** 116, 4094;
[10] Gilb, S.; Weis, P.; Furche, F.; Ahlrichs, R.; Kappes, M. M. *J. Chem. Phys.* **2002** 116, 4094; Walker, A. V. *J. Chem. Phys.* **2005** 122, 094310; Zhao, J.; Yang, J.; Hou, J. G. *Phys. Rev. B* **2003** 67, 085404; Olson. R. M.; Varganov, S.; Gordon, M. S.; Metiu, H.; Chretien, S.; Piecuch, P.; Kowalski, K.; Kucharski, S. A.; Musial, M. *J. Am. Chem. Soc.* **2005** 127, 1049; de Bas, B. S.; Ford, M. J.; Cortie, M. B. *J. Mol. Struc.* **2004** 686, 193; Mills, G.; Gordon, M. S.; Metiu, H. *J. Chem. Phys.* **2003** 118, 4198; Hkkinen, H.; Landman, U. *Phs. Rev. B* **2000** 62, 2287; Hkkinen, H.; Yoon, B.; Landman, U.; Li, X.; Zhai, H-J.; Wang, L-S. *J. Phys. Chem. A* **2003**, 107, 6168; Remacle, F.; Kryachko, E. S. *J. Chem. Phys.* **2005**, 122, 044304; Ford, M. J.; Hoft, R. C.; McDonagh, A. *J. Chem. Phys.* **2005** 109, 20387; de Bas, B. S.; Ford, M. J.; Cortie, M. B. *Theo. Chem.* **2004** 193, 686; Wang, J.; Jellinek, J.; Zhao, J.; Chen, Z.; King, B.; von Rague Schleyer, P. *J. Phys. Chem. A* **2005** 109, 9265.
[11] Bulusu, S.; Li, X.; Wang, L-S.; Zeng, X. C. *proc. Nat. Acad. Sci.* **2006** 103, 8326.
[12] Li, J.; Li, X.; Zhai, H-J.; Wang, L-S. *Science* **2003** 299, 864.
[13] Ercolessi, F.; Andreoni, W.; Tosatti, E. *Phys. Rev. Lett.* **1991** 66, 911.
[14] Cleveland, C. L.; Luedtke, W. D.; Landman, U. *Phys. Rev. Lett.* **1998** 81, 2036.
[15] Soulé de Bas, B.; Ford, M. J.; Cortie, M. B. *J. Phys. Condes. Mat.* **2006** 18, 55.
[16] Chacko, S.; Joshi, K.; Kanhere, D. G.; Blundell, S. A. *Phys. Rev. Lett.* **2004** 92, 135506.
[17] Joshi, K.; Krishnamurty, S; Kanhere, D. G. *Phys. Rev. Lett.* **2006** 96, 135703.
[18] Aguado, A.; Lopez, J. M. *Phys. Rev. Lett.* **2005** 94, 233401.
[19] Joshi, K.; Kanhere, D. G.; Blundell, S. A. *Phys. Rev. B* **2002** 66, 155329.
[20] Krishnamurty, S.; Joshi, K.; Kanhere, D. G.; Blundell, S. A. *Phys. Rev. B.* **2006** 73, 045419.
[21] Chuang, F.–C.; Wang, C. Z.; Ogut, S.; Chelikowsky, J. R.; Ho, K. M. *Phys. Rev. B* **2004** 69, 165408.
[22] Manninen, K.; Rytknen, A.; Manninen, M. *Eur. Phys. J.* **2004** 29, 39.
[23] Chacko, S.; Kanhere, D. G.; Blundell, S. A. *Phys. Rev. B* **2005** 71, 155407.
[24] Lee, M. S.; Chacko, S.; Kanhere, D. G. *J. Chem. Phys.* **2005** 123, 164310.
[25] Schmidt, M.; Kusche, R.; Kronmller, W.; von Issendorf,

B.; Haberland, H. *Phys. Rev. Lett.* **1997** 79, 99.

[26] Schmidt, M.; Kusche, R.; von Issendorf, B.; Haberland, H. *Nature (London)* **1998** 393, 238.

[27] Schmidt, M.; Donges, J.; Hippler, Th.; Haberland, H. *Phys. Rev. Lett.* **2003** 90, 103401.

[28] Haberland, H.; Hippler, T.; Dongres, J.; Kostko, O.; Schmidt, M.; von Issendorf, B. *Phys. Rev. Lett.* **2005** 94, 035701.

[29] Shvartsburg, A.; Jarrold, M. F. *Phys. Rev. Lett.* **2000** 85, 2530.

[30] Breaux, G. A.; Benirschke, R. C.; Sugai, T.; Kinnear, B. S.; Jarrold, M. F. *Phys. Rev. Lett.* **2003** 91, 215508.

[31] Breaux, G. A.; Hillman, D. A.; Neal, C. M.; Benirschke, R. C.; Jarrold, M. F. *J. Am. Chem. Soc.* **2004** 126, 8682.

[32] Breaux, G. A.; Neal, C. M.; Cao, B.; Jarrold, M. F. *Phys. Rev. Lett.* **2005** 94, 173401.

[33] Breaux, G. A.; Neal, C. M.; Cao, B.; Jarrold, M. F. *Phys. Rev. B* **2005** 71, 073410.

[34] S. Krishnamurty, S. Chacko, D. G. Kanhere, G. A. Breaux, C. M. Neal, and M. F. Jarrold Phys. Rev. B., **73**, 045406 (2006).

[35] C. M. Neal, A. K. Starace, M. F. Jarrold, K. Joshi, S. Krishnamurty, and D.G. Kanhere, Unpublished results.

[36] Payne, M. C.; Teter, M. P. ; Allen, D. C.; Arias, T. A.; Joannopoulos, J. D. *Rev. Mod. Phys.* **1991** 64, 1045.

[37] Nose, S. *Mol. Phys.* **1984** 52, 255.

[38] We have verified this for few temperatues in the present work and for several temperatues in other systems such as sodium, tin, silicon and gallium (unpublished work)
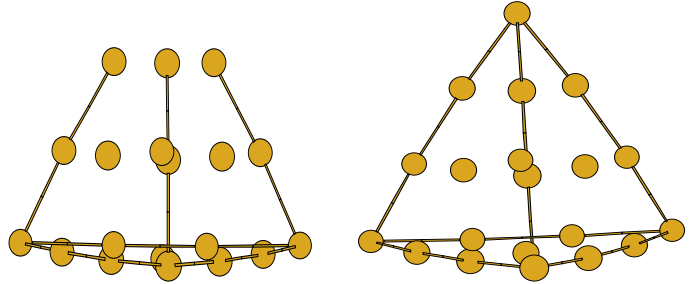
[39] Vanderbilt, D. *Phys. Rev. B* **1990** 41, 7892.

[40] *Vienna* Ab initio *simulation package*, Technische Universitt Wien **1999**; Kresse, G.; Furthmller, J. *Phys. Rev. B* **1996** 54, 11169.

[41] Chuang, F-c.; Wang, C.Z.; Ogut, S.; Chelokowsky, J.R.; Ho, K.M. *Phys. Rev. B* **2004** 69, 165408.

[42] Ferrenberg A. M.; Swendsen, R. H. *Phys. Rev. Lett.* **1988** 61, 2635; Labastie, P.; Whetten, R. L. Phys. Rev. Lett. **1990** 65, 1567.

[43] Kanhere, D. G.; Vichare, A.; Blundell, S. A. *Reviews in Modern Quantum Chemistry*, Edited by Sen, K. D., World Scientific, Singapore **2001**.

V.   TABLE OF CONTENTS GRAPHIC